Composites: Part A 102 (2017) 196–206

Contents lists available at ScienceDirect

Composites: Part A

journal homepage: www.elsevier.com/locate/compositesa

Understanding and predicting defect formation in automated fibre placement pre-preg laminates

Jonathan P.-H. Belnoue *, Tassos Mesogitis, Oliver J. Nixon-Pearson, James Kratz, Dmitry S. Ivanov, Ivana K. Partridge, Kevin D. Potter, Stephen R. Hallett

Bristol Composites Institute (ACCIS), Advanced Composites Collaboration for Innovation and Science, University of Bristol, University Walk, Bristol BS8 1TR, UK

ARTICLE INFO

Article history:
Received 25 May 2017
Received in revised form 2 August 2017
Accepted 4 August 2017
Available online 5 August 2017

Keywords:
Composite manufacturing simulation
Consolidation
Gaps and overlaps
Wrinkles

ABSTRACT

Fibre path defects are detrimental to the structural integrity of composite components and need to be minimised through process optimization. This requires understanding of the uncured pre-preg material, which is influenced by multiple process parameters, and sophisticated multi-scale modelling tools. Even though the capabilities of process modelling techniques have been improved over the past decades, the occurrence of localised wrinkles remains challenging to predict. One of the processes known to influence the formation of fibre path defects is the consolidation of laminates manufactured by automated fibre placement. The particular focus of this paper is to understand how out-of-plane wrinkles form during debulking and autoclave curing of laminates with embedded gaps and overlaps between the deposited tapes. Predictions are made using a novel modelling framework and validated against micro-scale geometry characterisation of artificially manufactured samples. The paper demonstrates the model's ability to predict consolidation defects for the latest generation of toughened pre-pregs.

1. Introduction

Current trends in composite manufacturing technologies for the aerospace industry are focussed on the automatic deposition of composite tapes and new multi-component materials systems, such as toughened prepregs, for improved component performance, damage tolerance or added functionality. The automation and material technologies enabling these advances have progressed much further than the capability to understand, predict, and optimise the manufacturing processes [1,2]. As a result, even though automatic fibre deposition technologies promise higher manufacturing rates, in practice lack of understanding of the pre-preg behaviour often leads to limited improvement in laydown rates. The complexities in processing present a high risk of defect generation and requires substantial investments in empirical optimisation.

Two of the main technologies for automated deposition of pre-preg material are Automated Tape Laying (ATL) and Automated Fibre Placement (AFP) [3–5]. The two techniques use very similar machines, consisting of a computer-controlled poly-articulated robot, with a placement head that lays bands of prepreg strips onto a mould in order to construct the layup (Fig. 1). ATL is employed to deliver wide prepreg tapes onto a surface whilst automatically removing the ply backing and is well adapted for the manufacturing of large parts of relatively simple geometry, e.g. an aircraft wing skin. AFP is similar to ATL but utilises narrow prepreg strips (the width of which can vary from $\frac{1}{8}''$ to $\frac{1}{2}''$), which are collimated on the head and then delivered together. As narrower tapes can steer over sharply curved surfaces better than wider tapes (that cannot be placed without buckling some of the fibres), AFP can be used to manufacture much more complex geometries e.g. wing spar C sections. In order to obtain good layup quality, it is essential to control all the process parameters (heating temperature, compaction pressure, placement speed, etc) [6–10] and the machine trajectories. Over the years, design rules have been implemented to optimise these trajectories for maximum final mechanical properties (stiffness and strength) of the component being constructed [11,12]. This is, however, insufficient to ensure the production of defect free components as the tolerance in the fibre placement head movement, steered fibres, and tow width variation all contribute to the introduction of gaps and overlaps within the laminate [3,13]. In addition, the optimisation process of the machine trajectory can itself be responsible for the introduction of further defects. What is not often taken into account in manufacturing practices and analysis of such defects is that the influence on final fibre path and ply geometry from gaps and overlaps is not their nominal as-deposited position, but a function of what happens to

* Corresponding author.
E-mail address: jonathan.belnoue@bristol.ac.uk (J.P.-H. Belnoue).

http://dx.doi.org/10.1016/j.compositesa.2017.08.008
1359-835X/

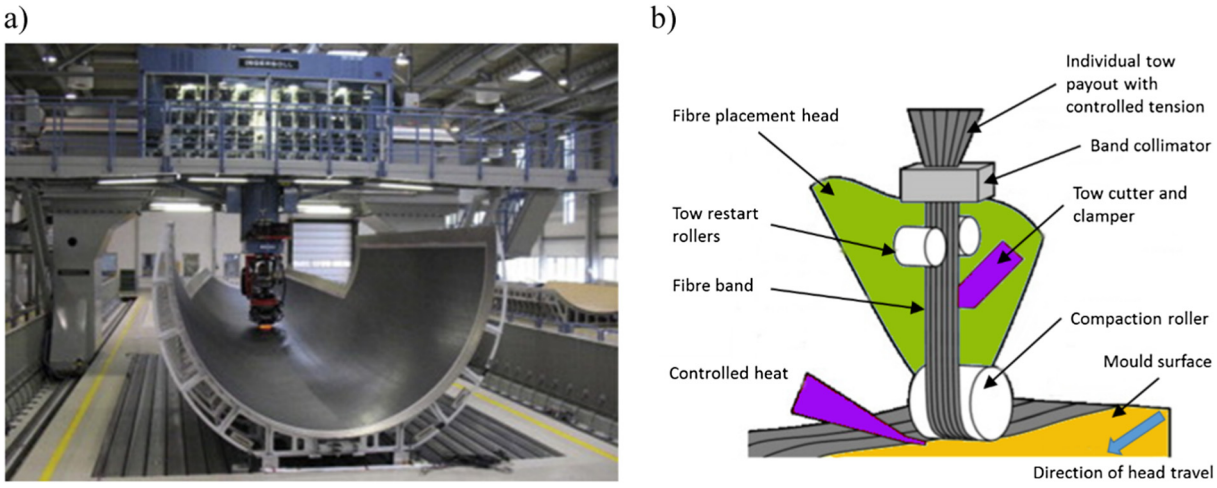

Fig. 1. (a) An AFP machine laying into a female mould [3] – (b) Automated fibre placement head, redrawn from [11].

the laminate in the subsequent processes, such as debulking or consolidation. The through-thickness deformation of the laminate with the gaps or overlapping tapes may lead to an additional fibre crimp or wrinkles, which can have a major impact on composite properties.

In recent years there have been a number of experimental and numerical studies carried out to predict and characterise the knockdown effect of gaps and overlaps on final mechanical properties of components manufactured by AFP. Amongst others, Sawicki and Minguet [14] have shown the reduction of compressive strength of samples with various distributions and sizes of gaps in 90° plies; Turoski [15] studied the knockdown effect under both tensile and compressive loading of isolated and interacting gaps with different stagger repeats; Croft et al. [16] investigated the effect of tensile, compressive and in-plane shear loading on the strength of laminates with a gap, an overlap and a half gap/overlap embedded in the through-thickness symmetry plane; and Elsherbini and Hoa [17] showed similar trends with respect to fatigue loading. More recently, Li et al. [18] generated sophisticated meshing tools which allowed them to easily create a series of finite element models with various combinations and permutations of gaps and overlaps. They were, then, able to systematically investigate the influence of defect size and distribution on the strength knockdown of the modelled specimens. The main conclusion of all these studies was that the introduction of gaps and overlaps during the layup process results (after consolidation and curing of the laminate) in the introduction of out-of-plane waviness of the load bearing 0° plies (i.e. wrinkles) adjacent to the gapped or overlapped layers and to local thickness variation which, in turn, are responsible for the decreased mechanical properties. This was later confirmed by Lan et al. [19,20] who showed that the use of a caul plate favours resin flow thus leading to reduced thickness variation and improved mechanical properties.

To limit the variation in strength of composite components made by automated manufacturing, it is absolutely imperative to establish more clearly how wrinkle severity and thickness variation can be reduced and, in the best case scenario, mitigate against it. With application to ATL of thermoplastic-based systems, Wang and Gutowski [21] studied analytically the possibility to remove (through processing) gaps and laps embedded in a lay-up. Although these studies were very informative, the authors only considered a very idealised geometry where the overlaps were described as cubical blocks of material superimposed with each other. Moreover, the evolution under processing conditions of only one embedded defect (i.e. one gap or one overlap) was considered. A real component manufactured by AFP, however, contains a very large number of different and complex combinations and permutations for gaps and overlaps, which can be of different sizes. A full exploration of the possibility to mitigate, through processing, defects in realistic engineering structure laid-up by AFP would therefore necessitate a very large and costly test plan. In comparison, composite process modelling offers the possibility to test a much larger range of possible combinations in a virtual sense and to optimise the processing parameters in order to minimise the defect sizes in a cured component. Process modelling could also advantageously replace or at least reduce empirical methods [18] and imaging techniques (which necessitates specimen/component manufacture) [22,23] for the generation of the internal ply geometry that is used as input to failure models. This would open the way for a fully virtual optimisation and strength prediction tool for composite components produced by AFP.

Most of the models available in the literature for the flow of resin in beds of reinforcement are based on Darcy's law [24,25]. These methods work very well to describe the evolution of the average thickness and fibre volume fraction in a large piece of prepreg when the edge effects can be neglected [26–29]. The principal modelling assumption is that bleeding flow (i.e. the pressure gradient causes resin flow relative to the fibre) is the main mechanism leading to the thickness variation of the laminate when processed. This is however not always fully representative as it has been known for a number of years [30] that squeezing flow (i.e. the laminate behaves as a highly viscous incompressible fluid) can also occur. Recently, Nixon-Pearson et al. [31] have shown that this can greatly affect the deformability of toughened thermoset prepreg under compaction. They highlighted that the smaller a prepreg volume with unconstrained boundaries (external or internal as in the case of tapes with gaps), the bigger the effect of squeezing flow on thickness evolution. This is important for the study of the consolidation of laminate produced by AFP as unconstrained narrow strips of prepreg and gapped and overlapped regions can locally affect the tape thickness to width ratio. This has been shown [31] to greatly influence the deformability of prepreg stacks. Hence, numerical tools for consolidation-induced deformation of laminate produced by AFP need to be able to capture these phenomena. The model recently proposed by Belnoue et al. [32] takes account of both bleeding and squeezing flow. It was shown to predict accurately the evolution of thickness and width over time of laminates subjected to complex pressure and pressure rate

cycles. It is also able to capture some of the interesting experimentally observed effects [31] such as the convergence to a compaction limit at high temperature and high pressure or the size effects observed in the through-thickness and transverse deformation of prepreg stacks under compaction.

The aim of the present study is to gain a better understanding of the way gaps and overlaps, which are introduced during automated prepreg layup, evolve during processing and promote the development of fibre path defects and thickness variation. As in-situ testing and observation of the evolution of the ply structure in the course of processing is not possible, another advantage of the modelling is that it gives information on how the plies move in relation to each other during the layup consolidation and resin cure. In the first part of this paper the model for the consolidation of toughened prepreg under processing conditions [32] is coupled to an existing cure simulation model, which allows to describe the full cure cycle. Validation of the updated models is given for structurally simple but internally complex test cases, comparing finite element (FE) predictions with experimental data. The second part of the paper focuses more closely on the processing of gaps and overlaps introduced during the layup process.

2. Modelling tools

The main novelty of the modelling approach is the use of the consolidation model for toughened prepreg presented in Belnoue et al. [32]. In order to be able to model the full cure cycle, the consolidation model is here coupled to cure simulation models that are well established in the literature [33,34]. The models are briefly summarized separately before their combination is presented in Section 2.3. The framework is then validated by simple test cases. The full list of the material parameters used throughout the study can be found at https://data.bris.ac.uk/data/dataset/x9rik93lx3tp1yeup4pe8kbti.

2.1. Consolidation model

The flow-compaction model used here follows directly from Belnoue et al. [32] where more details are given. Only the main model assumptions and equations are summarised. One of the model's main feature is that it is capable of accounting for both squeezing and bleeding flow. This is important for the modelling of toughened prepreg as they have been shown [31] to exhibit hybrid behavior between what would be expected from a thermoplastic based prepreg system (e.g. the variation of the material response with the tape width and thickness) and what is usually observed for thermosetting systems (e.g. the existence of a compaction limit).

The model uses the general thermodynamical framework proposed by Limbert and Middleton [35] for transversely isotropic solids. Although the framework was first formulated for the description of soft biological tissues (muscles), it is very relevant for the description of uncured prepreg as both materials are highly viscous and present one strong direction of anisotropy. It is assumed that the general thermodynamic potential, ψ, is additively decomposed into an elastic part (ψ^e which is related here to the deformation of fibres) and a viscous part (ψ^v related to the flow of matrix). Noting $\boldsymbol{C}$ the right Cauchy-Green deformation tensor, we can then express the second the Piola-Kirchhoff stress tensor as:

$$\boldsymbol{S} = \boldsymbol{S}^e + \boldsymbol{S}^v = 2\left(\frac{\partial \psi^e}{\partial \boldsymbol{C}} + \frac{\partial \psi^v}{\partial \dot{\boldsymbol{C}}}\right) \tag{1}$$

where $\dot{\boldsymbol{C}}$ denotes the derivative of $\boldsymbol{C}$ with respect to the time.

The expression of the elastic potential follows from Bonet and Burton [10].

$$\begin{aligned}\psi^e = {} & \frac{1}{2}\mu_T(I_1 - 3) - \mu_T \ln(J) + \frac{1}{2}\lambda(J-1)^2 \\ & + \left[(\mu_T - \mu_L) + \frac{\alpha}{4}\ln(J) + \frac{\beta}{8}(I_4 - 1)\right](I_4 - 1) + \frac{1}{2}(\mu_T - \mu_L) \\ & \times (I_5 - 1)\end{aligned} \tag{2}$$

where 1 is the second-order unit tensor, $I_1 = 1 : \boldsymbol{C}$, $I_2 = \frac{1}{2}[I_1^2 - (1 : \boldsymbol{C}^2)]$, $I_3 = J^2 = \det(\boldsymbol{C})$, $I_4 = \boldsymbol{N}_0 : \boldsymbol{C}$ and $I_5 = \boldsymbol{N}_0 : \boldsymbol{C}^2$. The material parameters α, β, λ, μ_T and μ_L in Eq. (2) can all be expressed as a function of the engineering constants. $\boldsymbol{N}_0$ is the structural tensor which characterizes the local directional properties of the material and is defined as $\boldsymbol{N}_0 = \boldsymbol{n}_0 \otimes \boldsymbol{n}_0$ (where $\boldsymbol{n}_0$ is the fibre orientation).

The expression for ψ^v follows from a phenomenological model proposed in [32] which builds on the work by Rogers [36] and Kelly [37]. Based on experimental results, the existence of a transition mechanism between squeezing (typically at low temperature and low pressure) and bleeding flow was postulated. This transition mechanism was thought to be related to what many authors have described in the past as locking, which corresponds to the point in time when the fibre bed reaches a configuration that is such that it cannot deform transverse to the fibres and transverse to the loading direction anymore. It was further assumed that after locking a change of direction of the resin flow between the fibres takes place, from transverse squeezing to bleeding. To ensure a smooth transition between the two mechanisms, squeezing flow theories were used in both cases. In other words, bleeding was mathematically represented as squeezing along the fibres.

Another consequence of this idealisation was that, unlike traditional flow models for thermosets prepreg which use Darcy's flow, the model assumed that the apparent viscosity of a piece of prepreg subjected to pure compressive loading could be multiplicatively decomposed into the product of a strain rate dependent term (assumed to behave as power law fluid) and a strain dependent term [37].

To capture the deformation of a prepregs with an anisotropic Stokes flow, a model would have to be defined at sub-ply resolution and a fine mesh through thickness of the plies would have to be used [31,38]. This is not practical for the simulation at a component scale. To overcome this difficulty a multiscale approach was used. As a result, the strain dependent term was further multiplicative decomposed into a component pertaining to the macro-scale deformation of the tape and a term (at the micro scale) expressing the evolution the inter-fibre channels. All this development finally leads to the formulation of two expressions for ψ^v. Prior to locking, the transverse behavior of the material is controlled by the viscous potential given in Eq. (3). After locking, ψ^v is expressed as in Eq. (4). In both these equations, J_2 is the strain rate invariant defined as $J_2 = \frac{1}{2}(1 : \dot{\boldsymbol{C}}^2)$.

$$\begin{aligned}\psi^v = {} & \left(\frac{w_0}{h_0}\right)^2 \frac{\sqrt{\chi_l}}{\chi_f} \frac{4Jke^b}{(a+2)} \left(\frac{1}{I_1^s}\right)^{-\frac{3}{2}} \left(\left(\frac{k}{\sqrt{I_1^s} - \frac{k}{\sqrt{\chi_f}}}\right)^2 + 3\chi_f\right) \\ & \times \left(\frac{1}{2\left[(I_1 - 1)^2 + 2I_3\right]}\right)^{\frac{a+2}{2}} J_2^{\frac{a+2}{2}}\end{aligned} \tag{3}$$

where $I_1^s = \frac{1}{2}\left((I_1 - 1) - \sqrt{(I_1 - 1)^2 - 4I_3}\right)$.

$$\psi^v = \left(\frac{l_0 w_0}{d h_0}\right)^2 \frac{\chi_l}{\chi_f} \frac{4Jke^b}{(a+2)} \left(\frac{1}{I_1^b}\right) \left(\frac{k}{\sqrt{I_1^b} - \frac{k}{\sqrt{\chi_f}}}\right)^2 \left(\frac{1}{2I_1^{b^2}}\right)^{\frac{a+2}{2}} J_2^{\frac{a+2}{2}} \tag{4}$$

where $I_1^b = I_1 - (1 + \chi_l)$.

Most of the terms in Eqs. (3) and (4) are known *a priori* as they are linked to the geometry of the tape and of the unit cell. l_0, w_0 and h_0 are the initial tape length (i.e. along the fibre direction), width and thickness respectively. Whilst χ_l and χ_f are the aspect ratios of a unit cell at locking and at the compaction limit respectively and d is the size of the fibres in the plane perpendicular to the fibre direction. Therefore, one of the most elegant aspects of the model is that it can describe the transverse behaviour of prepreg under processing conditions at constant temperature with 3 parameters only. The parameters a and b are two power law parameters controlling the behaviour of the rate dependent term of the apparent viscosity whilst the parameter k controls the size of the inter-fibre channels at the micro-scale. As shown in [32], these parameters can be easily determined by fitting straight lines through experimental data on a log–log plot of simple compaction tests performed on cruciform shaped samples.

2.2. Cure simulation model

A cure simulation model was developed and implemented using the commercial Finite Element Analysis code Abaqus/Standard. The simulation addresses the heat transfer effects occurring during the cure process and allows for quantification of the temperature and degree of cure evolution of the manufactured part. The model is three-dimensional and transient and has been applied to the Hexcel IM7/8552 prepreg material used in this study. The material properties depend on both the degree of cure and temperature and the material sub-models of cure kinetics, thermal conductivity and specific heat capacity were implemented in the user defined subroutine UMATHT. The heat transfer solution appropriate for simulating the cure process can be expressed by a three-dimensional energy balance combined with Fourier's heat conduction law and incorporating the exothermic heat generated due to the chemical reaction of the resin as follows [39]:

$$\rho c_p \frac{\partial T(\boldsymbol{r},T)}{\partial t} = \nabla \cdot \boldsymbol{K} \nabla T(\boldsymbol{r},T) + v_r \rho_r H_T \frac{da}{dt} \tag{5}$$

Here ρ and c_p are the density and the specific heat capacity of the composite, respectively, $\boldsymbol{K}$ is the thermal conductivity tensor, T the temperature, t and $\boldsymbol{r}$ the time and spatial coordinate and α the degree of cure. The rate of heat generation due to cure is expressed as the product of the resin volume fraction v_r, the density of the resin ρ_r, the total heat of reaction H_T and the cure reaction rate $d\alpha/dt$.

The cure kinetics model used for the resin system of this study is a combination of a nth order model and an autocatalytic model [34]. The specific heat capacity is defined based on the rule of mixtures for the relevant volume fraction of fibres and matrix whilst a geometry-based model is implemented to compute the thermal conductivity [34]. The fibres' specific heat capacity and thermal conductivity present a linear dependence on temperature [33], whilst the resin specific heat capacity and thermal conductivity depend on both degree of cure and temperature [34].

2.3. Thermo-mechanical model

A coupled three-dimensional transient thermo-mechanical model was developed by coupling the consolidation model and the cure simulation model presented in Sections 2.1 and 2.2. Again, the coupled model was developed within the implicit FE package Abaqus/Standard. A staggered solution approach is adopted (see Fig. 2). The heat transfer analysis is carried out first, followed by the mechanical analysis. As described in Section 2.2 the heat transfer solution is coded within a UMATHT subroutine yielding the evolution of temperature and degree of cure of the laminate. This information is then passed to a UMAT subroutine where the mechanical model described in Section 2.1 is coded. The coupling between the heat transfer solution and the consolidation model is carried out by expressing the consolidation phenomenological parameters a, b and k as a function of temperature [32]. The thermal and chemical strains occurring during the process cycle are taken into account by considering the thermal expansion [40] and cure shrinkage coefficients [41] of the material. In addition, the fact that consolidation stops at gelation, is deployed numerically by assigning a very large apparent viscosity η_{app} after the resin gels, i.e. when the instantaneous degree of cure α reaches the degree of cure at gelation α_{gel}. The degree of cure at gelation α_{gel} for the resin system of this study is 0.33 [41].

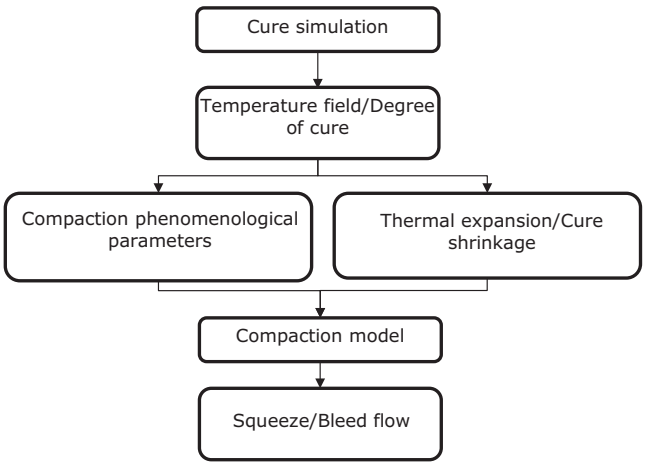

Fig. 2. Schematic representation of the thermo-mechanical model.

2.4. Model validation

2.4.1. Cure simulation model validation

To validate the cure simulation model, an 18 mm thick flat panel was cured within an autoclave. The flat panel was placed on a 10 mm aluminium tooling plate, bagged up and sealed before testing. A K-type thermocouple was mounted at the centre of the laminate in order to record the temperature evolution of the laminate during the process. The nominal cure profile [42] of the 8552 resin system was applied whilst the lay-up of the laminate was $[0/90]_{37s}$. The cure of an 18 mm thick flat panel was then modelled using the developed cure simulation model and the results were compared with the experimental data. The widely accepted material properties of aluminium were applied to the tool. Hence, the thermal conductivity and the specific heat capacity were set at 120 [W/m/^{0}C] and 960 [J/kg/^{0}C], respectively, whereas the density was fixed at 2700 kg/m^3. The heat convection coefficients for the given autoclave were determined experimentally using lumped mass thermal analysis. It was shown that the heat convection coefficients of the top and bottom surfaces were 27.3 and 31.7 [W/m^2/K], respectively. In addition, adiabatic conditions were applied at the lateral walls of the laminate assuming no heat loss due to the high width to thickness ratio.

Fig. 3 presents the temperature evolution and the degree of cure at the centre of the laminate. As it can been seen there is a very good agreement between the experimental data and simulation results implying that the cure simulation model developed is able to simulate the heat transfer phenomena occurring during the cure process of the material system of this study successfully. The temperature lag between the centre of the laminate and the autoclave air is due to the heat convection between the autoclave and the

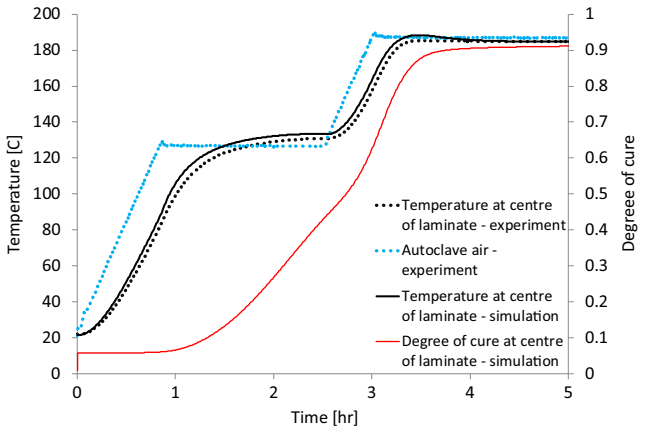

Fig. 3. Cure of 18 mm thick IM7/8552 flat panel; evolution of temperature and degree of cure at the centre of the laminate.

laminate as well as due to the low thermal conductivity in the through the thickness direction.

2.4.2. Thermo-mechanical model validation

A series of experiments were carried out in order to validate the developed thermo-mechanical model. The cruciform specimen developed in [31] was used for the layup and geometry. Two different configurations of 16 plies laminates were studied; cross-ply (CP), $[0/90]_8$ and blocked-ply (BP), $[90_4/0_4/90_4/0_4]$ as shown in Fig. 4a. The experimental testing was carried out using an Instron 8801 universal testing machine with temperature controlled hot plates transferring the temperature and pressure profile to the samples (see Fig. 4b). The nominal temperature and pressure profile from the manufacturers recommended cure cycle were applied. The coupled thermo-mechanical model presented in Section 2.3 was used to model the compaction of the two samples and the results were compared with the experimental data. Prescribed temperature boundary conditions were applied to all the bottom and top nodes of the model representing the hot plates, whilst prescribed pressure was applied to all the top nodes representing the applied pressure. Fig. 5a depicts the heat transfer results for the two case studies. The evolution of both the degree of cure and temperature is identical between the two configurations since the layup does not affect the heat transfer in the through-the thickness direction. In addition, there is no temperature and degree of cure distribution within the laminates due to the fact that the laminates are relatively thin (2 mm). Furthermore, there is no heat loss between the hot plates and the laminates since they are in direct contact. In the beginning of the cycle consolidation effects dominate, leading to a considerable thickness reduction until the thickness reaches a plateau at the middle of the second ramp where the resin has gelled and cure shrinkage strains start to develop. This phenomenon is accurately captured by the model since the degree of cure at the middle of the second ramp has reached the α_{gel} as shown in Fig. 5a. The increase of temperature during the second ramp results in a slight increase in thickness caused by thermal expansion effects followed by a slight decrease due to resin chemical shrinkage. During the second dwell there is no variation in thickness whereas there is a slight thickness reduction at the end of the cycle during cool-down caused by thermal contraction. Overall, there is a quite good agreement between the experimental data and the simulation results (see Fig. 5b) implying that the coupled model is capable of capturing the thickness evolution during consolidation, accounting for the cessation of compaction at gel and also thermal expansion effects. Furthermore, it is shown that the model can capture the layup size effects; the CP laminate shows less thickness reduction than the BP laminate due to the fact that the apparent viscosity is proportional to the width to thickness ratio rendering the CP laminate considerably more viscous [31].

3. Wrinkle formation – AFP gaps and overlaps

3.1. Sample design and experimental procedure

In order to validate further the flow model and coupled approach and to gain a better understanding of the mechanisms involved in the consolidation of gaps and overlaps introduced during the Automated Fibre Placement lay-up process, a sample with a

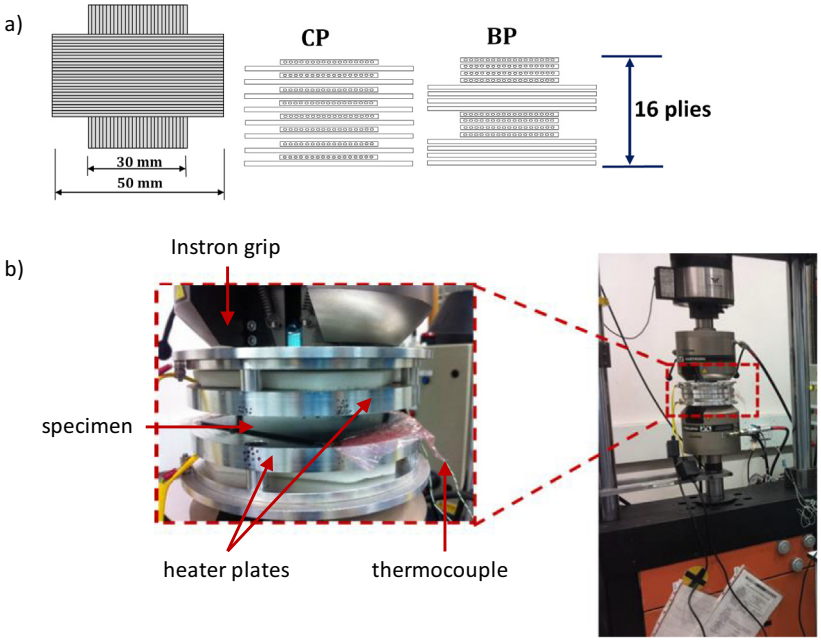

Fig. 4. (a) Schematic representation of cross-ply (CP) and blocked-ply (BP) samples. – (b) Experimental set-up.

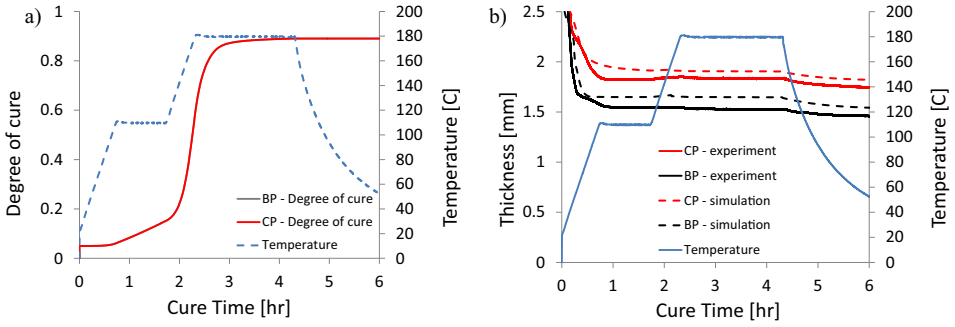

Fig. 5. (a) Heat transfer solution for cross ply and blocked ply laminate, (b) coupled solution for cross ply and blocked ply laminate.

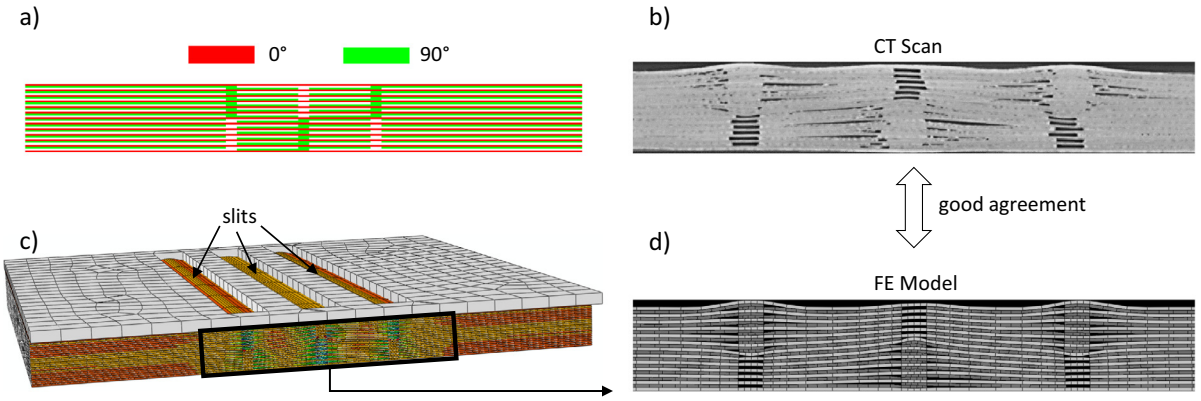

Fig. 6. Gaps and overlaps specimen (a) Ply book, (b) CT scan after vacuum consolidation, (c) Initial geometry for the FE analysis, obtained through forming of the plies initially laid-up "flat" (see Fig. 6a), (d) Realistic internal ply geometry in the FE model of the uncompacted sample after the forming phase.

purposely severe combination of gaps and overlaps was designed and manufactured from broadgoods IM7/8552. As illustrated in Fig. 6(a), the sample is a 100 mm × 100 mm × ~6 mm with a cross-ply layup in which 3 defect areas are embedded in the 90° plies. Each of these defect areas is made of 5 gaps stacked on top of each other, directly above a stack of 5 overlaps. In the central defect region, the order of the gaps and overlaps regions are the opposite to the outer two regions. All the defects are 2 mm wide, which is of the same order of magnitude as defects introduced by an AFP process. Fig. 6(b) shows a CT scan of the centre-line of a specimen that has been vacuum-bagged and then oven-cured for imaging purposes.

The samples described above were submitted to two different types of thermomechanical loading. First, isothermal experiments were carried out at 70 °C. The laminates were loaded at a rate of 2.333 kPa·s^{-1} to 1 bar, 3 bars and 7 bars respectively and then maintained at these levels of pressure over 1 h. An Instron 8801 universal testing machine with temperature controlled hot plates was used to apply the temperature and pressure profile to the samples. The obtained samples were then fully cured in an oven (without pressure) and micrographs were taken. The second test program used the same equipment to load the sample under the pressure and temperature cycle recommended by the manufacturer [42], mimicking an autoclave curing process.

3.2. Isothermal loading

Although there is no composite manufacturing process that uses the load and temperature program applied in the isothermal tests, the levels of load and temperature were carefully chosen to be meaningful from a composite processing perspective. Thus, 70 °C is close to the hot debulking temperature, 1 bar is equivalent to vacuum pressure, 3 bar is close to the pressure applied by an AFP roller and 7 bar is the autoclave pressure. These tests were carried out with 2 main objectives:

- to give further validation for the flow model presented in Belnoue et al. [32] for larger samples with more complex internal ply geometry
- to gain more understanding of the way gaps and overlaps consolidate and interact during the consolidation process and the mechanisms involved.

FE models of the tests described above were set up in Abaqus/Standard. A ply-by-ply modelling approach was used. The necessity to start with an accurate geometry of the uncompacted specimen led to the definition of a two-step modelling procedure. The first step consisted in the forming of the plies laid-up flat, as in Fig. 6(a). As illustrated in Fig. 6(c), this was done using a rigid plate that was moved down in order to progressively bring the plies into contact with each other. The 3 bumps observed on the sample top at the position of each of the defect areas (see Fig. 6b), were reproduced by placing 3 slits in the forming plate through which the material can penetrate. The good agreement between the FE model and a CT scan of a specimen that had been vacuum bagged and then oven cured with no pressure applied on the specimen (as can be seen comparing Fig. 6(d) with Fig. 6(b)) validated the choice of the forming procedure. The second part of the analysis consisted in the compaction of the samples between 2 rigid plates. In all the simulations, the material model for pre-preg was that from [32]. Custom-developed algorithms allowed for automatic mesh generation and material property assignment from direct reading of the ply book. Single integration point elements with hourglass control were used, with one element per ply in the thickness direction.

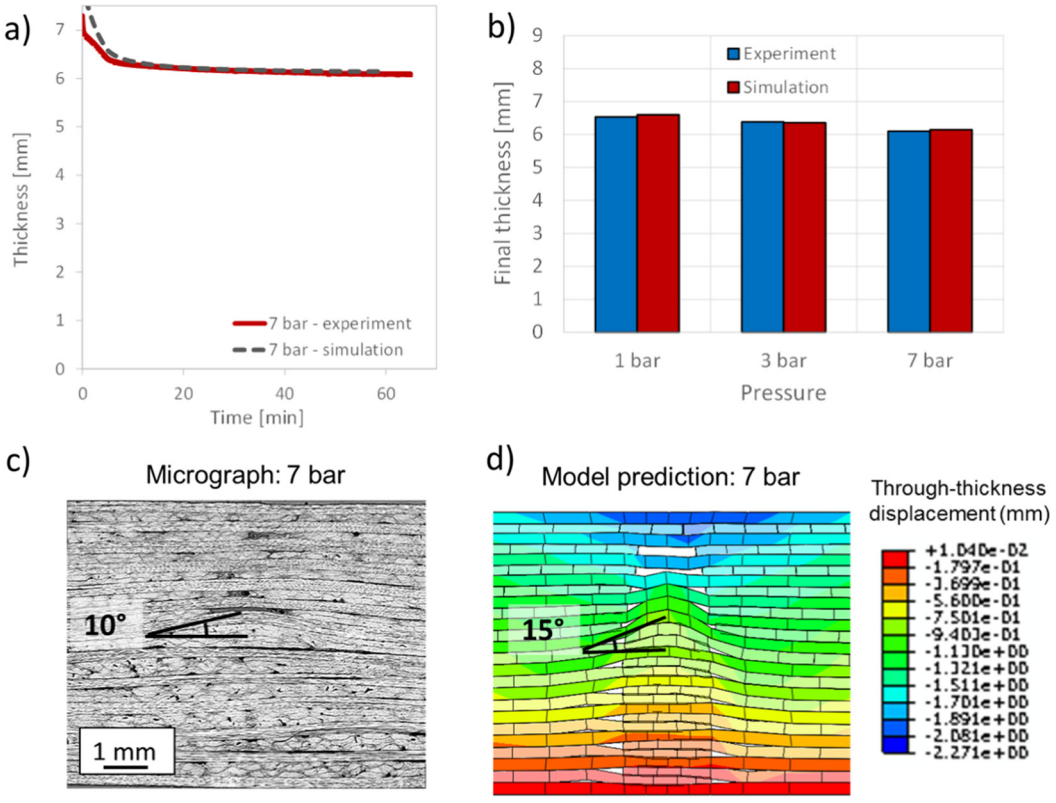

Fig. 7. Comparison of FE predictions with experimental results for the isothermal experiments. (a) Thickness vs Time evolution of the sample tested a 7 bar, (b) Experimental and predicted thicknesses of the samples tested at respectively 1 bar, 3 bar and 7 bar, (c) Micrograph of the defect area in the middle of the sample at 7 bar, (d) FE prediction for the internal ply geometry around a central defect region of the sample with a 7 bar applied pressure.

As illustrated by Fig. 7(a) and (b), the predicted thickness evolution for the 3 levels of pressure compared very well with those measured experimentally. Similarly, good agreement is obtained when comparing samples' micrographs (Fig. 7c) with the final ply geometry predicted by the model (Fig. 7d). Both the ply thickness and the level of filling of the gaps originally introduced in the sample are very well captured by the model. However, the predicted wrinkle angle (~15° in the sample tested at 7 bars) is more severe than what is observed in the micrographs (~10°). There are several possible explanations for this. Firstly, the model does not take account of the resin once it has bled out of the fibre bed into the gap. This potentially resists the development of the wrinkle. Secondly, as can be seen in Fig. 6(b) and contrary to what is assumed in the model, the gaps (in the real samples) are not perfectly aligned. This makes it more difficult for the wrinkle to develop. Lastly, as it has been shown in the context of dry fibre fabric forming [43], the bending stiffness can considerably affect the severity of the wrinkle. The present model was formulated for prediction of consolidation, with the value of the bending stiffness taken directly from Sjölander et al. [44]. There a cantilever bending test was performed at 70 °C on a piece of prepreg made from epoxy resin and IM fibres. The bending stiffness in an FE model of the test was adjusted until the predictions matched the experimental results. Sjölander et al. [44] reported the difficulty to calibrate this property properly. This suggests that, in the future, more effort should be dedicated to more clearly understanding the bending behavior of prepreg sheets under processing conditions.

Fig. 8, shows the initial configuration and the final geometry predictions of the internal ply geometry around the central wrinkle for the 3 different pressure levels. As expected, most of the variation of the thickness happens between 0 and 1 bar. The figure highlights the existence of two competing mechanisms in the way the gaps originally introduced within the laminates are filled. Upon compaction, the gaps can either close due to the overlaps falling into the gaps (the wrinkle then becomes steeper) or they can be filled laterally due to squeezing flow (this prevents the wrinkle angle from increasing as can be seen at the position marked 'a' on the sample loaded to 7 bars). Including capabilities for squeezing flow into the model also allowed to take account of the higher compressibility of the overlapped areas. It can be clearly seen in the 7 bar sample that these regions are compacted nearly twice as much as the single plies. This was also observed on the micrographs of the samples (Fig. 7c).

3.3. Full cure cycle

The second set of experiments, where the same apparatus was used to submit the sample to the manufacturer's recommended pressure and temperature cycle, was used to validate the two-step coupled thermo-mechanical model proposed in Section 2.3. The same material parameters as in Section 2.4.2 and the same initial mesh as Section 3.2 were used. First, the temperature history at every gauss point in the model was calculated during the heat transfer analysis (which uses the UMATHT subroutine). This showed that, the temperature distribution through the thickness of the laminate was negligible with a slight temperature overshoot, in the order of two degrees at the beginning of the second dwell. The temperature field history was then given as an input to the mechanical analysis (which uses the UMAT subroutine). Fig. 9(a) depicts the thickness evolution of the laminate, whilst Fig. 9(b) presents a micrograph and the corresponding simulation result. It can be observed that the coupled model is able to predict the thickness evolution of the laminate during consolidation accurately. Comparison of the simulation results with the micrograph

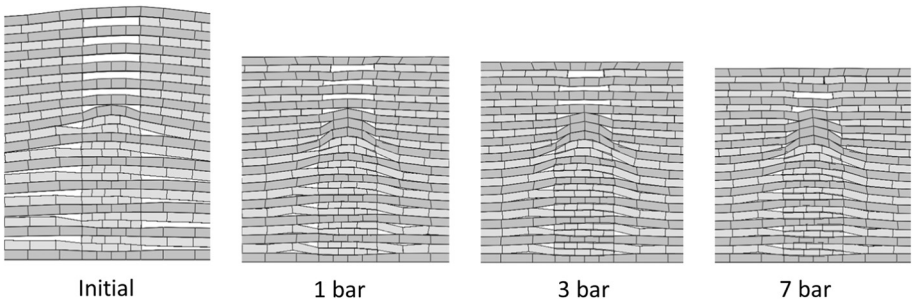

Fig. 8. Prediction for the internal ply geometry around the central wrinkle at different level of pressure.

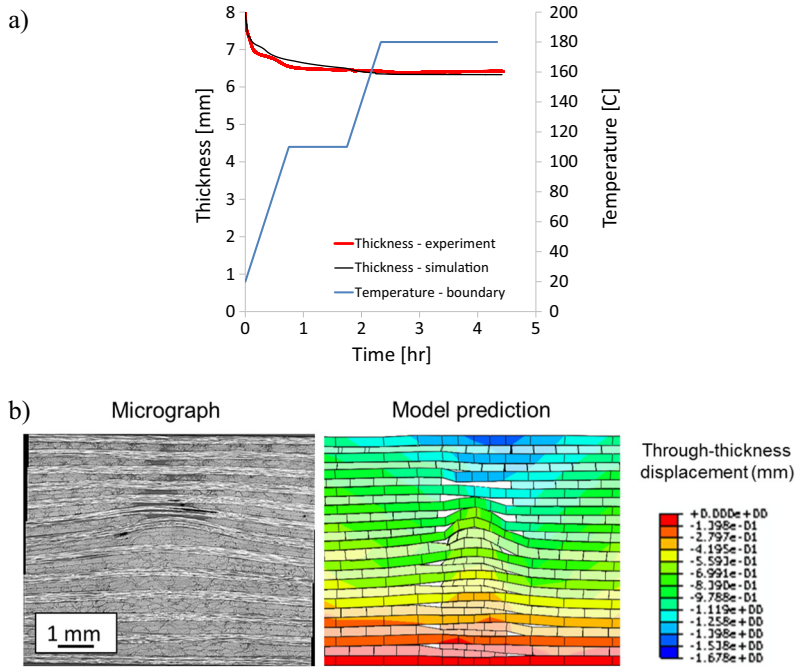

Fig. 9. Gaps and overlaps coupled solution (a) Thickness evolution (b) Model prediction comparison with sample micrographs for the internal ply geometry around the central wrinkle.

shown in Fig. 9(b) indicates that the coupled model predicts the morphology of the manufactured part successfully, including the filling of the gaps as well as the formation and position of the wrinkle. As with the isothermal experiments, the model slightly over-predicts the magnitude of the formed wrinkle.

4. Complex distribution of gaps and overlaps

Although very informative about the mechanisms playing a role in the consolidation of gaps and overlaps, the study presented in the previous section was a rather simple and forced case compared to a real lay-up created by AFP. For example, the probability to see, 5 gaps facing exactly opposite to 5 overlaps is quite low. Moreover, in the industry AFP machines tends to be set-up so that they leave only gaps or only overlaps in the layup. The model's ability to predict the effect of consolidation and curing on more realistic lay-ups with more complex distribution and a greater number of gaps and overlaps is presented.

Two different lay-up configurations were modelled (see Fig. 10). As for the previous section, a cross-ply configuration was adopted. Both lay-ups had the same defect distribution but one of them only contained gaps whilst the other one only had overlaps. The defect width was 2 mm, which is consistent with the size of the defects

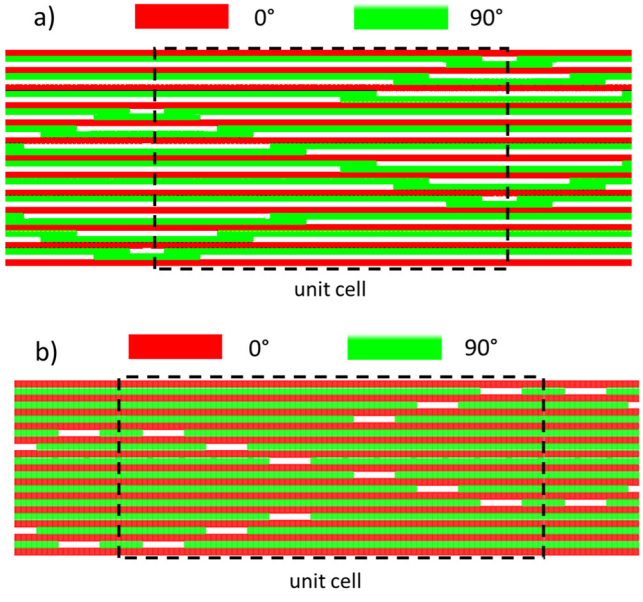

Fig. 10. Ply books for the layups with a complex distribution of manufacturing defects. (a) 100% overlaps – (b) 100% gaps.

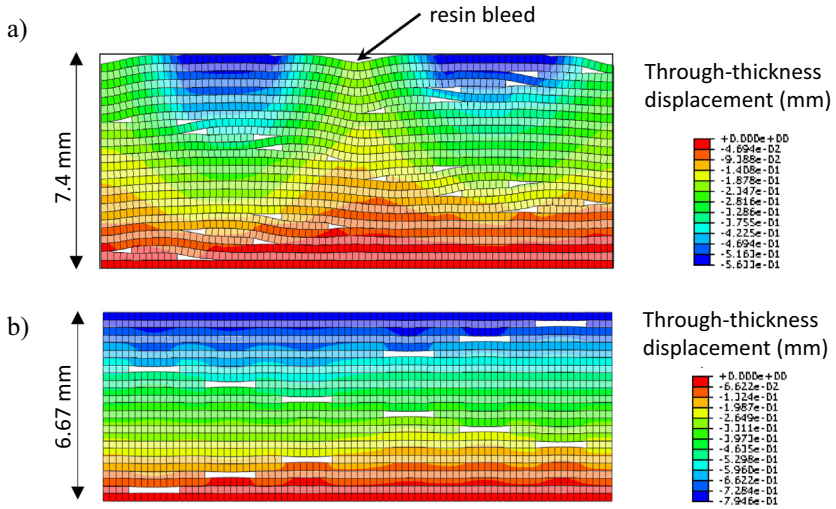

Fig. 11. Final internal geometry for the layups with a complex distribution of manufacturing defects: Consolidation and cure under hard tooling. (a) 100% overlaps – (b) 100% gaps.

introduced in an AFP process. The same modelling procedure as the one described in the previous section was used except that the laminate that contained only gaps did not need to be formed. The samples were assumed to be infinitely long in the two in-plane directions therefore only a representative unit cell with fully constrained edges was modelled. Temperature and pressure boundary conditions were applied to simulate the samples being subjected to the cure cycle. It was assumed that the samples were consolidated between 2 aluminium plates, which were modelled as rigid bodies. The material parameters were the same as those used throughout the paper, given in Section 2.

The results of the analysis are illustrated in Fig. 11. Comparing the final internal geometry of the lay-up where only overlaps were introduced and the case with 100% gaps reveals significant differences between the 2 cases. The sample with 100% overlaps is about 0.7 mm thicker. In addition, there is significantly more fibre waviness created in this sample. This is important from a design point of view as the level of fibre waviness can, as discussed in the introduction, impact the sample load carrying capacity greatly, whilst the sample thickness has implications for assembly tolerances. In the model there is a 'void' formed at the top surface where the plies have deformed. In reality, this would be filled by resin bleed, which can not be captured by the analysis. This may however be an artefact of the excessive ply bending, which was observed in the examples in Section 3. The difference in thickness observed between the two cases is partly due to the sample with embedded overlaps being originally thicker, as a result of the introduction of extra material in the overlapped regions. However as can be seen in Fig. 11, it is also due to the samples with embedded gaps being able to compact more. This can mainly be explained by the fact that in the samples with embedded overlaps the plies are continuous (i.e. infinitely long). It was shown in [31] that the higher the square of the ply thickness to width (i.e. dimension in the direction perpendicular to the fibre direction) ratio, the greater the amount of squeezing flow and the more the material is able to compact. It can also be remarked that, contrary to what might be expected, there is almost no waviness in the samples with embedded gaps. This is because the samples gels very early on in the cure cycle, which results in the structure being "frozen" and unable to deform any more.

It is also interesting to remark that unlike what was observed in the case presented in Section 3 where a sample with a deliberately

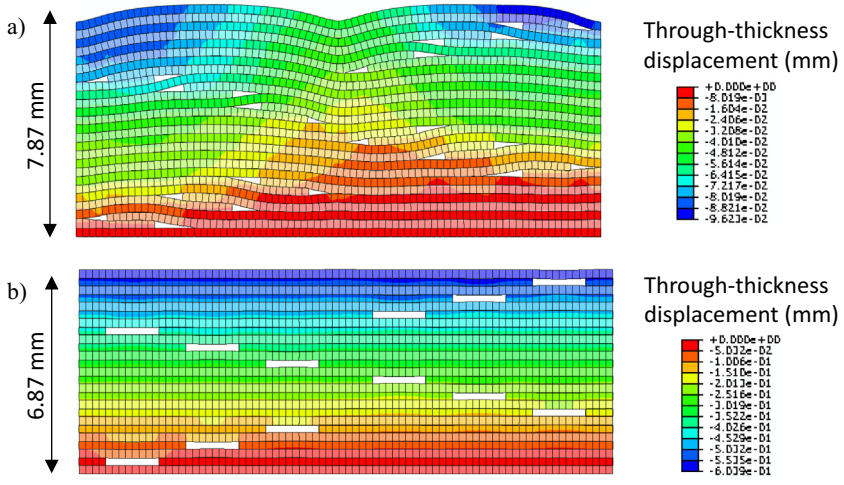

Fig. 12. Final internal geometry for the layups with a complex distribution of manufacturing defects: Consolidation and cure with soft tooling. (a) 100% overlaps – (b) 100% gaps.

bad combination of gaps and overlaps was analysed, lateral squeezing flow does not seem to help to fill up the gaps (see Fig. 11b). This is because in the present case the ply thickness to width ratio is much smaller, thus limiting the ability of the material to squeeze. In this example, counterintuitively, the introduction of gaps in the 90° plies compared to the overlaps has helped to increase the overall fibre volume fraction of the sample, since it is able to consolidate more easily. In the case of the overlaps, they cause the top tooling to be held up, preventing overall consolidation of the un-overlapped regions.

Finally, in order to demonstrate the model's ability to study different manufacturing cases, an analysis where the hard top tooling was replaced by a soft vacuum bag was carried out (in practice a homogeneous pressure was applied to the top of the samples). The result of the analysis is illustrated in Fig. 12. In the sample with embedded overlaps (see Fig. 12(a)), soft tooling results in a lot less compaction than what was observed with hard tooling (see Fig. 11 (a)). This is the result of the applied pressure being non-homogeneously distributed when hard tooling is used. In fact, in the hard tooling case, the compacting plate is only in contact with the bumps at the surface of the sample. As a result, the force applied at the top of the tool is distributed over a much smaller area and the actual pressure applied on some parts of the lay-up is much greater than the external pressure applied to the rigid tool. This also results in much reduced waviness in the lay-up consolidated and cured under hard tooling. This is in good agreement with the observations made by Lan et al. [19,20] when studying the effect of tooling on the resistance to failure of samples containing gaps and overlaps.

5. Conclusion

This work has presented new insight into the formation of fibre path defects arising in AFP manufactured laminates, through experimental observations and predictive modelling. To achieve this a new multi-scale and multi-physics modelling framework for composite processing, based on a consolidation model proposed by Belnoue et al. [32] has been defined. Using a method presented by Johnston et al. [33], the consolidation model was coupled to a heat transfer model for accurate description of the full cure cycle. Validation of the newly introduced models was first given for very simple test cases comparing FE predictions with experimental data. This model was then applied to analysis of the processing of specimens with gaps and overlaps introduced during the layup process and for the understanding of how these layup defects can evolve into fibre path defects.

A specimen was designed with a purposely "bad" combination of gaps and overlaps of realistic sizes. This magnified the effect of the different mechanisms participating in the gaps and overlaps consolidation and closure, thus facilitating their identification. Samples were laid-up and processed in 2 different ways: isothermally, subjected to 3 different pressure levels and following the manufacturer's recommended cure cycle (mimicking that of an autoclave). Micrographs of samples and measurement of the final thickness allowed further model validation. This highlighted the model's ability to capture the mechanisms leading to the final ply configuration. Upon compaction, the gaps can either close due to the overlaps falling into the gaps or be filled laterally due to squeezing flow. Comparison between the model predictions and this set of experiments also highlighted the necessity for further investigation, in the future, at the effect of the ply bending stiffness on the wrinkle severity and to explore new methods to take this into account more accurately within the modelling framework proposed here.

In the last part of the paper it was shown how the newly developed numerical tool can be used to predict the evolution of the internal geometry and ply configuration of components containing much more complex and realistic arrangements of gaps and overlaps. The emphasis has been put on predicting the effect of tooling on the samples' final internal geometry. It highlighted the effect of the plies' dimensions on the ability of the layup to compact. As much as 10% difference in the predicted thickness was obtained between the thickest specimen that contained the most severe waviness (100% overlaps with soft tooling) and the thinnest one (100% gaps with hard tooling).

The new predictive capabilities developed here opens the way towards process optimisation and defect mitigation in parts manufactured by automated prepreg lay-up. For example, a sensitivity analysis on the material and processing parameters would help to limit the amount of part re-work and scrap by improving the general understanding of how manufacturing conditions affect the quality of the laminate. In addition, the modelling framework presented in this study can be enhanced to predict residual stress and shape distortion occurring during the cure so that all the phenomena occurring during the manufacturing process of composites can be captured. It also holds potential to be used as part of a virtual framework for the prediction of the mechanical properties of engineering components made from composite materials, including the formation and effects of fibre path defects.

Acknowledgements

This work has been funded by the UK Engineering Physical Sciences Research Council (EPSRC) Centre for Innovative Manufacturing in Composites project "Defect Generation Mechanisms in Thick and Variable Thickness Composite Parts – Understanding, Predicting and Mitigation" (DefGen), [EP/I033513/1]. Data for the cure simulations models, including equations and materials parameters can be found at https://data.bris.ac.uk/data/dataset/x9rik93lx3tp1yeup4pe8kbti.

References

[1] Zobeiry N, Forghani A, Li C, Gordnian K, Thorpe R, Vaziri R, et al. Multiscale characterization and representation of composite materials during processing. Philosophical Transact Royal Soc London A: Mathemat, Phys Eng Sci 2016;374 (2071).
[2] Baran I, Cinar K, Ersoy N, Akkerman R, Hattel JH. A review on the mechanical modeling of composite manufacturing processes. Archiv Computat Methods Eng 2016;1–31.
[3] Lukaszewicz DHJA, Ward C, Potter KD. The engineering aspects of automated prepreg layup: History, present and future. Compos B Eng 2012;43 (3):997–1009.
[4] Grimshaw MN, Grant CG, Luna Diaz JM. Advanced Technology Tape Laying for Affordable Manufacturing of Large Composite Structures. 2001.
[5] Marsh G. Automating aerospace composites production with fibre placement. Reinf Plast 2011;55(3):32–7.
[6] Lukaszewicz DHJA, Potter KD, Eales J. A concept for the in situ consolidation of thermoset matrix prepreg during automated lay-up. Compos B Eng 2013;45 (1):538–43.
[7] Chinesta F, Leygue A, Bognet B, Ghnatios C, Poulhaon F, Bordeu F, et al. First steps towards an advanced simulation of composites manufacturing by automated tape placement. Int J Mater Form 2014;7(1):81–92.
[8] Bur N, Joyot P, Ghnatios C, Villon P, Cueto E, Chinesta F. On the use of model order reduction for simulating automated fibre placement processes. Adv Model Simulat Eng Sci 2016;3(1):1–18.
[9] Lichtinger R, Hörmann P, Stelzl D, Hinterhölzl R. The effects of heat input on adjacent paths during Automated Fibre Placement. Compos A Appl Sci Manuf 2015;68:387–97.
[10] Gangloff Jr JJ, Simacek P, Sinha S, Advani SG. A process model for the compaction and saturation of partially impregnated thermoset prepreg tapes. Compos A Appl Sci Manuf 2014;64:234–44.
[11] Debout P, Chanal H, Duc E. Tool path smoothing of a redundant machine: application to automated fiber placement. CAD Comput Aided Design 2011;43 (2):122–32.
[12] Shirinzadeh B, Foong CW, Tan BH. Robotic fibre placement process planning and control. Assemb Automat 2000;20(4):313–20.
[13] Lukaszewicz DHJA. Considerations for Automated Layup of Carbon-Fibre Thermoset Preimpregnates, (PhD Thesis). 2011.
[14] Sawicki AJ, Minguet PJ. Effect of intraply overlaps and gaps upon the compression strength of composite laminates. Collection of Technical Papers

- AIAA/ASME/ASCE/AHS/ASC Structures, Structural Dynamics and Materials Conference 1998. p. 744–54.
[15] Turoski LE. Effects of manufacturing defects on the strength of toughened carbon/epoxy prepreg composites. Montana State University-Bozeman; 2000.
[16] Croft K, Lessard L, Pasini D, Hojjati M, Chen J, Yousefpour A. Experimental study of the effect of automated fiber placement induced defects on performance of composite laminates. Compos A Appl Sci Manuf 2011;42(5):484–91.
[17] Elsherbini YM, Hoa SV. Experimental and numerical investigation of the effect of gaps on fatigue behavior of unidirectional carbon/epoxy automated fiber placement laminates. J Compos Mater 2016.
[18] Li X, Hallett SR, Wisnom MR. Modelling the effect of gaps and overlaps in automated fibre placement (AFP)-manufactured laminates. Sci Eng Compos Mater 2015;22(2):115–29.
[19] Lan M, Cartié D, Davies P, Baley C. Microstructure and tensile properties of carbon-epoxy laminates produced by automated fibre placement: Influence of a caul plate on the effects of gap and overlap embedded defects. Compos A Appl Sci Manuf 2015;78:124–34.
[20] Lan M, Cartié D, Davies P, Baley C. Influence of embedded gap and overlap fiber placement defects on the microstructure and shear and compression properties of carbon–epoxy laminates. Compos A Appl Sci Manuf 2016;82:198–207.
[21] Wang EL, Gutowski TG. Laps and gaps in thermoplastic composites processing. Compos Manufact 1991;2(2):69–78.
[22] Mukhopadhyay S, Jones MI, Hallett SR. Tensile failure of laminates containing an embedded wrinkle; numerical and experimental study. Compos A Appl Sci Manuf 2015;77:219–28.
[23] Mukhopadhyay S, Jones MI, Hallett SR. Compressive failure of laminates containing an embedded wrinkle; Experimental and numerical study. Compos A Appl Sci Manuf 2015;73:132–42.
[24] Hubert P, Poursartip A. A review of flow and compaction modelling relevant to thermoset matrix laminate processing. J Reinf Plast Compos 1998;17(4):286–318.
[25] Niaki SA, Forghani A, Vaziri R, Poursartip A. A two-phase integrated flow-stress process model for composites with application to highly compressible phases. Mech Mater 2017;109:51–66.
[26] Hubert P, Poursartip A. Method for the direct measurement of the fibre bed compaction curve of composite prepregs. Compos A Appl Sci Manuf 2001;32(2):179–87.
[27] Hubert P, Vaziri R, Poursartip A. A two-dimensional flow model for the process simulation of complex shape composite laminates. Int J Numer Meth Eng 1999;44(1):1–26.
[28] Gutowski TG, Cai Z, Bauer S, Boucher D, Kingery J, Wineman S. Consolidation experiments for laminate composites. J Compos Mater 1987;21(7):650–69.
[29] Li M, Tucker Iii CL. Modeling and simulation of two-dimensional consolidation for thermoset matrix composites. Compos - Part A: Appl Sci Manufact 2002;33(6):877–92.
[30] Hubert P, Poursartip A. Aspects of the compaction of composite angle laminates: an experimental investigation. J Compos Mater 2001;35(1):2–26.
[31] Nixon-Pearson O, Belnoue JPH, Ivanov DS, Potter KD, Hallett SR. An experimental investigation of the consolidation behaviour of uncured prepregs under processing conditions. J Compos Mater 2017;51(13):1911–24.
[32] Belnoue JPH, Nixon-Pearson OJ, Ivanov D, Hallett SR. A novel hyper-viscoelastic model for consolidation of toughened prepregs under processing conditions. Mech Mater 2016;97:118–34.
[33] Johnston A. An integrated model of the development of process-induced deformation in autoclave processing of composite structures. University of British Columbia; 1997.
[34] Van Ee D, Poursartip A. HexPly 8552 MATERIAL PROPERTIES DATABASE for use with COMPRO CCA and Raven. 2009.
[35] Limbert G, Middleton J. A transversely isotropic viscohyperelastic material Application to the modeling of biological soft connective tissues. Int J Solids Struct 2004;41(15):4237–60.
[36] Rogers TG. Squeezing flow of fibre-reinforced viscous fluids. J Eng Math 1989;23(1):81–9.
[37] Kelly PA. A viscoelastic model for the compaction of fibrous materials. J Text Inst 2011;102(8):689–99.
[38] Ghnatios C, Abisset-Chavanne E, Binetruy C, Chinesta F, Advani S. 3D modeling of squeeze flow of multiaxial laminates. J Nonnewton Fluid Mech 2016;234:188–200.
[39] Shojaei A, Reza Ghaffarian S, Mohammad Hossein Karimian S. Three-dimensional process cycle simulation of composite parts manufactured by resin transfer molding. Compos Struct 2004;65(3–4):381–90.
[40] Ersoy N, Garstka T, Potter K, Wisnom MR, Porter D, Stringer G. Modelling of the spring-in phenomenon in curved parts made of a thermosetting composite. Compos A Appl Sci Manuf 2010;41(3):410–8.
[41] Garstka T, Ersoy N, Potter KD, Wisnom MR. In situ measurements of through-the-thickness strains during processing of AS4/8552 composite. Compos A Appl Sci Manuf 2007;38(12):2517–26.
[42] Hexcel®. HexPly® 8552 Epoxy Marix Product Data. 2014.
[43] Boisse P, Hamila N, Vidal-Sallé E, Dumont F. Simulation of wrinkling during textile composite reinforcement forming. Influence of tensile, in-plane shear and bending stiffnesses. Compos Sci Technol 2011;71(5):683–92.
[44] Sjölander J, Hallander P, Åkermo M. Forming induced wrinkling of composite laminates: A numerical study on wrinkling mechanisms. Compos A Appl Sci Manuf 2016;81:41–51.